Investigation of Inverse Bremsstrahlung Heating Driven by Broadband Lasers

Xiaoran Li¹, Jie Qiu¹, Liang Hao¹‡, Chen Wang²§, Lifeng Wang¹, Shiyang Zou¹

- ¹ Institute of Applied Physics and Computational Mathematics, Beijing 100094, People's Republic of China
- 2 Shanghai Institute of Laser Plasma, CAEP, Shanghai 201899, People's Republic of China

26 November 2025

Abstract. Broadband lasers have become a key strategy for mitigating laser plasma instabilities in inertial confinement fusion, yet their impact on collisional inverse bremsstrahlung (IB) heating remains unclear. Using one dimensional collisional particle-in-cell simulations, we systematically examine the effect of bandwidth induced temporal incoherence on IB absorption in Au plasmas. The simulations are first benchmarked against classical absorption theory, verifying that the implemented Coulomb collision model accurately reproduces the theoretical IB heating rate. A direct comparison of the electron temperature evolution in the broadband and monochromatic cases shows that, although spectral broadening introduces transient picosecond scale oscillations in the heating rate driven by stochastic intensity fluctuations, the long term averaged heating and net IB absorption remain essentially unchanged.

Keywords: laser driven inertial confinement fusion, broadband lasers, inverse bremsstrahlung heating

‡ Corresponding author: hao_liang@iapcm.ac.cn

§ Corresponding author: wch11@163.com

1. Introduction

Broadband lasers have recently attracted increasing attention in inertial confinement fusion (ICF) as a promising approach to mitigate laser plasma instabilities (LPI). By introducing frequency spread and temporal incoherence, broadband laser disrupts the phase matching among resonant waves and effectively suppresses the coherent amplification of parametric instabilities. Recent experiments on both the Kunwu and PHELIX laser facilities have demonstrated effective mitigation of SBS in CH targets with a modest bandwidth of 0.5%-0.6% [1-4, suggesting that spectral broadening can play a crucial role in achieving LPI-free ignition schemes. Meanwhile, extensive computational studies have further examined how processes such as stimulated Raman scattering (SRS), two plasmon decay (TPD), stimulated Brillouin scattering (SBS), and cross beam energy transfer (CBET) depend on the bandwidth and intensity of broadband lasers, thereby extending our understanding of broadband driven laser plasma interactions [5–10].

In contrast, a closely related question has received far less attention: whether introducing laser bandwidth also alters the collisional inverse bremsstrahlung (IB) absorption that dominates energy deposition in the subcritical plasmas relevant to ICF. Since IB heating depends on both the instantaneous laser intensity and the evolving plasma state [11], the stochastic sub-picosecond fluctuations inherent to broadband light could, in principle, could modify the temporal structure of collisional energy deposition even when the long time mean intensity is fixed. This motivates a central question: does spectral broadening intrinsically change the physics of IB heating, or does it simply modulate the instantaneous intensity that drives an otherwise identical absorption process? Clarifying this issue is essential for evaluating the extent to which broadband driven plasmas differ from monochromatic ones in both kinetic and fluid descriptions.

In this work, we use collisional particle-in-cell (PIC) simulations to isolate the role of bandwidth induced temporal incoherence on IB heating, keeping the mean intensity, central frequency, and plasma parameters fixed. We first verify that the collisional absorption computed by the PIC model is consistent with classical theory, confirming the correct implementation of the Coulomb collision operator. We then compare the temporal evolution of the electron temperature T_e and the heating rate dT_e/dt under monochromatic and broadband illumination. The results show that while the broadband laser produces short time oscillations in the heating rate due to its stochastic intensity modulation, the long term evolution and overall absorption efficiency remain nearly identical to those of the

monochromatic case.

2. Simulation Model and Parameters

2.1. Simulation setup

The influence of laser bandwidth on the energy absorption and electron heating of high-Z plasmas was investigated using the one-dimensional, three-velocity (1D3V) particle-in-cell (PIC) code EPOCH [12]. Binary Coulomb collisions among all species were included through the Nanbu Monte Carlo algorithm [13, 14], allowing for self consistent modeling of collisional absorption.

The simulated target was a spatially uniform Au plasma with an electron density of $n_e = 0.1n_c$, where n_c is the critical density corresponding to a laser wavelength of 530 nm. The initial electron and ion temperatures were $T_e = 200 \text{ eV}$ and $T_i = 10 \text{ eV}$, respectively. The Au charge state was fixed at Z = 50, and the ion density was set to $n_{\rm Au} = n_e/50$ to ensure quasineutrality. Each cell contained 10,000 electron and 200 ion macroparticles with equal particle weights, which was found to improve the accuracy of electronion collisional energy exchange. The total simulation domain was $L = 300 c/\omega_0$, which was discretized into 4500 spatial cells, corresponding to a resolution of $\Delta x \approx 0.067 \, c/\omega_0$, where ω_0 is the laser frequency with a wavelength of 530 nm. Two convolutional perfectly matched layers [15], each consisting of 80 grids, are applied at both ends of the domain to absorb outgoing electromagnetic waves. The laser, with an intensity of $I_0 = 5 \times 10^{14} \,\mathrm{W/cm^2}$, was injected from the left boundary and propagated into the plasma with open field and particle boundaries at both ends. The total simulation time was 35 ps, sufficient to capture both the transient and steady state heating phases.

Two types of laser fields were considered: (1) a monochromatic laser with a wavelength of 530 nm, and (2) a broadband laser centered at 530 nm with a relative bandwidth of 0.6%. The broadband field was modeled using the multi-frequency beamlet approach, where N=100 discrete frequency components with equal amplitudes and random initial phases were superposed to reproduce a flat top spectrum. This approach has been widely adopted in broadband laser-plasma interaction studies and has been shown to accurately reproduce temporal incoherence while remaining computationally efficient [16–18].

The main diagnostic of interest is the spatially averaged electron temperature $T_e(t)$, which characterizes the cumulative effect of laser energy absorption. The diagnostic region is chosen as the central portion of the plasma $(100-200 \, c/\omega_0)$, where boundary effects and field reflections are negligible. Since the IB heating rate in the present regime exceeds the rate of col-

lisional thermal relaxation, the velocity distribution naturally deviates from a Maxwellian and exhibits a super-Gaussian form—an expression of the Langdon effect [19,20]. For each recorded snapshot, the electron velocity distribution function is extracted and fitted with a super-Gaussian profile

$$f(v) \propto \exp[-(v/v_{\rm th})^m],$$

from which the effective temperature T_e is derived. Because the primary focus of this study is the temporal evolution of T_e rather than the variation of the exponent m, the fitting parameter is fixed at m=2.6, which corresponds to the value obtained from fitting the electron velocity distribution at the final stage of the simulation. Within the total simulation duration of 35 ps, the electron temperature is evaluated every $\Delta t = 10^4/\omega_0 \approx 2.8$ ps from successive distribution snapshots, allowing a detailed comparison between broadband and monochromatic laser heating dynamics.

2.2. Verification of collisional inverse-bremsstrahlung (IB) absorption

To validate the reliability of the collisional heating model, we benchmarked the inverse bremsstrahlung (IB) absorption obtained from our EPOCH runs against the classical collisional absorption theory.

For a homogeneous plasma with electron–ion collision frequency ν_{ei} , the group velocity of the pump is $v_g = c\sqrt{1 - n_e/n_c}$, and the collisional attenuation coefficient reads [11]

$$\mu_c = \nu_{ei} \frac{n_e/n_c}{v_g}. \tag{1}$$

Assuming Beer–Lambert decay of the pump envelope, the pump intensity varies as $I(x) = I_0 \exp(-\mu_c x)$. The transmitted intensity after a propagation distance L is $T = \exp(-\mu_c L)$, giving the theoretical absorption

$$A_{\rm th} = 1 - \exp(-\mu_c L). \tag{2}$$

The collision frequency ν_{ei} used to generate the theory curve is computed as [21],

$$\nu_{ei} = \frac{4\sqrt{2\pi} \, n_i Z^2 e^4 \ln \Lambda}{(4\pi\varepsilon_0)^2 \, 3 \, m_e^{1/2} \, T_e^{3/2}},\tag{3}$$

where n_i and Z are the ion density and charge state, T_e is the electron temperature, and $\ln \Lambda$ is the Coulomb logarithm.

In simulations, the IB absorption $A_{\rm PIC}$ is obtained from the spatial evolution of the pump envelope. Let $E_y(x,t)$ be the transverse field; its cycle averaged envelope $E_{\rm env}(x)$ is extracted via Hilbert transform. To avoid boundary effects, the upstream and downstream diagnostic windows are placed well inside the plasma, covering $x/L \in [0.05, 0.15]$ and $x/L \in [0.85, 0.95]$. The

absorption is computed directly from the averaged field amplitudes in the upstream and downstream regions as

$$A_{\text{PIC}} = 1 - \frac{\langle E_{\text{env}}^2 \rangle_{x \in [0.85L, 0.95L]}}{\langle E_{\text{env}}^2 \rangle_{x \in [0.05L, 0.15L]}}.$$
 (4)

Time averaging over many optical cycles is used to reduce statistical noise. Note that a constant incident laser intensity is used in this test.

For a consistent comparison, the theoretical absorption is evaluated over the same effective propagation distance as used in the PIC diagnostic. Since the mean positions of the two windows correspond approximately to $x_{\rm in} \simeq 0.1L$ and $x_{\rm out} \simeq 0.9L$, the theoretical absorption is therefore given by

$$A_{\text{th}}^{(\text{win})} = 1 - \exp[-\mu_c (x_{\text{out}} - x_{\text{in}})] = 1 - \exp(-\mu_c 0.8L), (5)$$

which represents the expected attenuation between the same effective regions used in the PIC diagnostic.

Figure 1 compares the simulated absorption $A_{\rm PIC}$ with the theoretical prediction $A_{\rm th}$ over a wide range of electron–ion collision frequencies ν_{ei} . In the simulations, ν_{ei} is varied by adjusting the electron temperature T_e , using the same plasma configuration and domain setup described in section 2.1. The corresponding theoretical values $A_{\rm th}(\nu_{ei})$ are evaluated using identical parameters for direct comparison. The test cases cover an electron temperature range of $T_e = 200 - 1500$ eV, which fully encompasses the heating conditions investigated in this work. The EPOCH results exhibit excellent agreement with the theoretical curve, demonstrating that collisional energy absorption is accurately captured in the simulations.

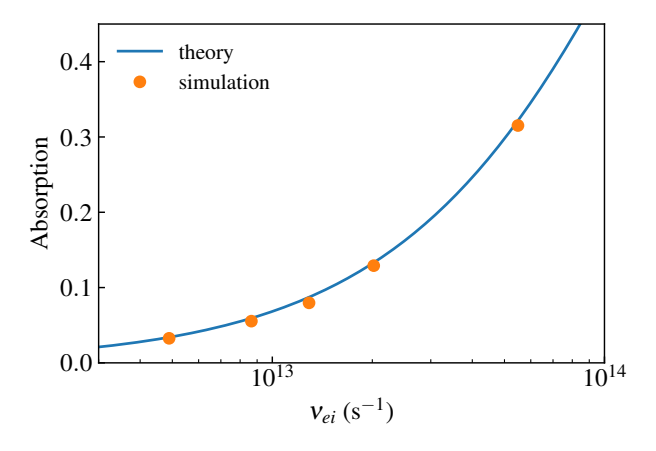


Figure 1: Comparison between the simulated and theoretical inverse bremsstrahlung (IB) absorption. The simulated absorption $A_{\rm PIC}$ obtained from EPOCH is plotted against the theoretical prediction $A_{\rm th}$ as a function of the electron–ion collision frequency ν_{ei} .

3. Simulation results and discussion

3.1. Temporal intensity modulation of broadband lasers

Since inverse bremsstrahlung depends on the instantaneous laser intensity, understanding how the broadband field fluctuates in time provides the basis for interpreting its heating behavior. Figure 2 illustrates the temporal evolution of the instantaneous and time averaged electric field intensity E^2 for the monochromatic (E_m) and broadband (E_b) lasers at the same mean intensity of $I_0 = 5 \times 10^{14} \text{ W/cm}^2$. As shown in figure 2(a), the monochromatic laser exhibits a nearly constant envelope, whereas the broadband laser consists of a sequence of short, randomly varying wave packets, whose instantaneous intensity fluctuates strongly in time. The duration of these wave packets corresponds approximately to the laser coherence time, which characterizes the timescale over which the field remains phase correlated. The coherence time of a broadband laser with a fractional bandwidth of $\Delta\omega/\omega_0 = 0.6\%$ can be estimated as [16, 22]

$$\tau_c \simeq \frac{2\pi}{\Delta\omega} = \frac{2\pi}{0.006\,\omega_0} \approx 0.29 \text{ ps},$$

where ω_0 is the central frequency corresponding to $\lambda_0 = 0.53 \ \mu\text{m}$. Each intensity spike in figure 2(a) therefore represents a coherence burst lasting on the order of $\tau_c \approx 0.29$ ps.

Although the instantaneous broadband intensity fluctuates strongly on the sub-picosecond scale, its time averaged value converges to that of the monochromatic laser once the averaging window significantly exceeds τ_c , as shown in figure 2(b). Averaging over a relatively short window of $\Delta t = 10\tau_c \approx$ 2.9 ps still leaves noticeable residual oscillations, reflecting partial temporal correlation across several coherence bursts. When the averaging window is extended to $\Delta t = 50\tau_c \approx 14.5 \,\mathrm{ps}$, these residual modulations are strongly suppressed and the averaged intensity becomes nearly indistinguishable from the monochromatic level. Consistently, the broadband E^2 averaged over the full 35 ps simulation is almost identical to that of the monochromatic case, confirming that the mean intensity is preserved despite rapid subpicosecond fluctuations. For a fixed averaging window, increasing the bandwidth further shortens τ_c , thereby increasing the number of uncorrelated wave packets sampled within Δt and producing an even smoother and more stable averaged intensity profile.

3.2. IB heating dynamics with monochromatic and broadband lasers

Figure 3 shows the temporal evolution of the electron temperature T_e and its growth rate dT_e/dt in a

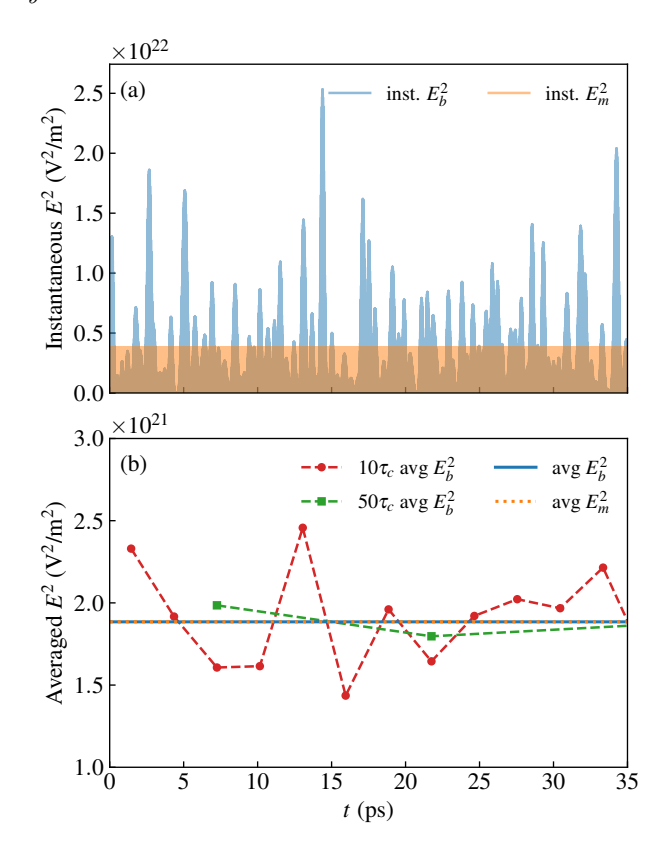


Figure 2: Temporal evolution of the instantaneous and averaged E^2 for broadband (E_b) and monochromatic (E_m) lasers at equal mean intensity, illustrating how different averaging windows $(10\tau_c)$ and $(50\tau_c)$ smooth the broadband intensity fluctuations.

homogeneous Au plasma irradiated by monochromatic and broadband lasers. Throughout the simulations, no significant laser–plasma instabilities such as SRS, TPD, or SBS are observed, implying that electron heating is governed almost entirely by IB absorption.

For both the monochromatic and broadband cases, the electrons absorb laser energy through IB, causing the temperature T_e to rise rapidly at early times before gradually approaching a quasi saturated value of approximately 1.25 keV, as shown in figure 3(a). As T_e increases, the IB absorption coefficient decreases due to the reduction of the electron–ion collision frequency, which leads to a continuous decline in the heating rate dT_e/dt , illustrated in figure 3(b). At sufficiently high temperatures, the effective absorption rate becomes negligible, and the plasma approaches local thermal equilibrium.

Although the overall trends of $T_e(t)$ are similar for the broadband and monochromatic cases, noticeable differences arise on picosecond time scales. During the first ~ 6 ps, the broadband laser produces a slightly higher electron temperature than the monochromatic one. Afterward, the broadband T_e temporarily

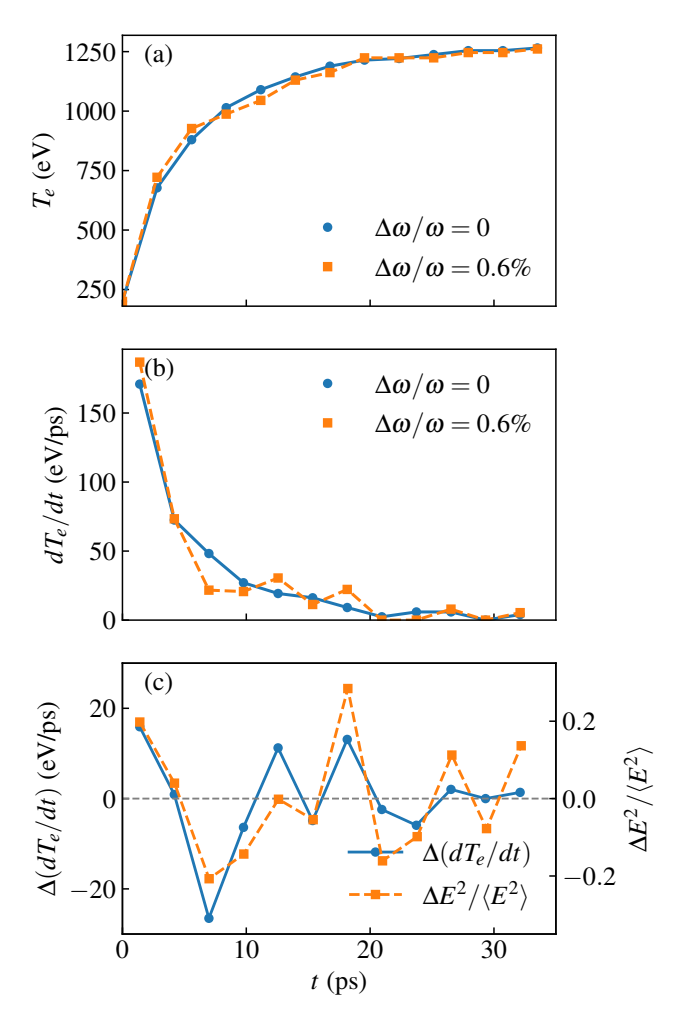


Figure 3: Temporal evolution of (a) the electron temperature T_e , (b) its temporal growth rate dT_e/dt , and (c) the difference in heating rate between broadband and monochromatic cases $\Delta(dT_e/dt)$ compared with the normalized laser intensity variation $(E_{\rm b}^2 - \langle E_{\rm m}^2 \rangle)/\langle E_{\rm m}^2 \rangle$. Here T_e is evaluated every $\Delta t = 10^4/\omega_0 \approx 2.8\,{\rm ps},\, (E_{\rm b}^2 - \langle E_{\rm m}^2 \rangle)/\langle E_{\rm m}^2 \rangle$ is estimated with the same time window.

falls below the monochromatic curve before both gradually converge at later times. The monochromatic heating rate dT_e/dt decreases almost monotonically throughout the simulation, whereas the broadband case exhibits distinct oscillations in dT_e/dt despite following the same overall downward trend. To clarify the relation between the dT_e/dt fluctuations and the temporal intensity modulation of the broadband field, we compare the difference in heating rate between the two cases, $\Delta(dT_e/dt)$, with the normalized laser intensity variation $(E_b^2 - \langle E_m^2 \rangle)/\langle E_m^2 \rangle$, as shown in figure 3(c). Here, $T_e(t)$ is sampled every $10^4/\omega_0 \approx 2.8$ ps, and the intensity variation is evaluated on the same 2.8 ps window for direct comparison. The

two curves exhibit nearly synchronous oscillations, demonstrating that the transient modulation of dT_e/dt directly follows the time averaged fluctuations of the laser intensity.

To interpret the origin and temporal evolution of these oscillations, it is useful to introduce a characteristic time scale for electron heating,

$$\tau_{\rm IB}(t) \equiv \frac{U_e(t)}{Q_{\rm abs}(t)} = \frac{\frac{3}{2} n_e k_B T_e(t)}{\alpha_{\rm IB}(T_e) I(t)} \simeq \frac{T_e(t)}{dT_e/dt}, \quad (6)$$

where $\tau_{\rm IB}$ is called the characteristic IB heating time, $U_e(t) = \frac{3}{2}n_e k_B T_e(t)$ is the electron internal energy density, $Q_{abs}(t)$ is the absorbed laser power density, $\alpha_{\rm IB}(T_e)$ is the temperature dependent IB absorption coefficient per unit length (m^{-1}) , I(t) is the instantaneous laser intensity, n_e is the electron number density, and k_B is the Boltzmann constant. Physically, $\tau_{\rm IB}$ represents the plasma response time to collisional laser heating, that is, the time required for the electron temperature to undergo a significant fractional change due to IB absorption. This timescale depends on both the laser and plasma parameters: higher laser intensity or stronger electron—ion collisions (larger $\alpha_{\rm IB}$) shorten $\tau_{\rm IB}$, while higher electron temperatures, which reflect both reduced collisionality and increased internal energy, tend to produce a longer $\tau_{\rm IB}$.

The heating dynamics can be understood as a competition between the laser coherence time τ_c and the collisional heating time $\tau_{\rm IB}$, where the former characterizes the temporal fluctuation of the laser intensity and the latter governs the response of the electron temperature. When $\tau_{\rm IB}$ is comparable to τ_c , the plasma can respond rapidly enough to follow the short time intensity oscillations of the broadband field, producing visible fluctuations in dT_e/dt . In the early stage of the present simulation, $\tau_{\rm IB}$ is estimated to be ~ 3 ps, about ten times the laser coherence time $(\tau_{\rm IB} \sim 10\tau_c)$. During this period, the heating rate difference $\Delta(dT_e/dt)$ exhibits pronounced oscillations that closely track the averaged intensity modulation on a comparable 2.8 ps timescale, as shown in figure 3(c). This indicates that even when $\tau_{\rm IB}$ exceeds τ_c by an order of magnitude, the plasma still partially responds to the residual low frequency intensity variations that persist over several coherence intervals. As the plasma heats up and dT_e/dt decreases, $\tau_{\rm IB}$ increases rapidly and exceeds $200\tau_c$ after about 20 ps, over which the driving field intensity averaged across this timescale becomes nearly constant. At this stage, the plasma response is determined primarily by the time averaged intensity, and the oscillations in $\Delta(dT_e/dt)$ are strongly suppressed. Hence, the electron plasma behaves as a low pass temporal filter with a cutoff determined by $\tau_{\rm IB}$: intensity components varying on timescales much shorter than $\tau_{\rm IB}$ are smoothed out by collisional energy exchange, leaving the net IB heating essentially insensitive to laser bandwidth. The chosen diagnostic window of 2.8 ps remains shorter than $\tau_{\rm IB}$ throughout the simulation, ensuring sufficient temporal resolution to capture the detailed evolution of $T_e(t)$.

Looking back at the overall trend, the broadband and monochromatic $T_e(t)$ curves gradually converge at later times, differing by less than 0.3% at t =This indicates that although temporal 35 ps. incoherence introduces short time fluctuations in dT_e/dt , the overall collisional absorption efficiency remains essentially unchanged. This behavior arises because both cases share the same central frequency and density ratio (n_e/n_c) ; hence, the absorption coefficient μ_c defined in equation (1) is governed by the electron-ion collision frequency given in equation (3). The latter depends primarily on the plasma state rather than on the spectral bandwidth. Therefore, the observed short term differences result from temporal intensity modulation rather than from intrinsic changes in the inverse bremsstrahlung cross section, explaining why the net heating efficiency and final equilibrium temperature are nearly identical for both monochromatic and broadband illumination. These findings further imply that, for radiation hydrodynamic simulations concerned with evolution on hundreds of picoseconds or longer [23, 24], broadband illumination can be safely modeled using an equivalent monochromatic source, since bandwidth induced modulation does not leave lasting imprints on the collisional heating history.

4. Conclusions

In this study, we have investigated the influence of broadband laser illumination on collisional inverse bremsstrahlung (IB) heating in Au plasmas. Using one dimensional collisional particle-in-cell simulations, we isolated the effects of bandwidth while keeping the mean laser intensity, central frequency, and plasma parameters fixed. The simulations were first benchmarked against classical absorption theory, confirming that the implemented collision model accurately reproduces the theoretical IB heating rate over a wide range of electron temperatures.

A detailed comparison of the electron temperature evolution was performed between the broadband and monochromatic cases. In both scenarios, $T_e(t)$ rises rapidly at early times and then gradually approaches a saturated value. The heating rate dT_e/dt in the monochromatic case decreases almost monotonically, whereas the broadband case exhibits picosecond-scale oscillations that track the stochastic intensity fluctuations of the pump. These oscillations, however, are transient and vanish when averaged over durations much longer than the coherence time. The persistence

or suppression of these fluctuations is governed by the relation between the characteristic IB heating time $\tau_{\rm IB}$ and the laser coherence time τ_c : when $\tau_{\rm IB} \gg \tau_c$, the plasma effectively averages over rapid intensity modulations, leading to a long term absorption efficiency that is indistinguishable from that of monochromatic illumination. This indicates that, for radiation hydrodynamic simulations that typically evolve over hundreds of picoseconds or longer, the broadband laser can be effectively modeled as an equivalent monochromatic source of the same mean intensity.

Acknowledgments

This work was supported by the National Natural Science Foundation of China (Grant Nos. 12505268, 12275032, 12205021 and 12075227) and the China Postdoctoral Science Foundation (Grant No. 2024M764280).

Data availability statement

The data cannot be made publicly available upon publication because the cost of preparing, depositing and hosting the data would be prohibitive within the terms of this research project. The data that support the findings of this study are available upon reasonable request from the authors.

References

- [1] Kang N, Zhao Y, Lei A, Liu H, Li F, Xu G, An H, Xiong J, Wang R, Xie Z, Fang Z, Wang W, Ji L, Zhou S, Hu G, Li J, Wang L, Gao Y, Huang X and Fu S 2025 Nuclear Fusion 65 026042
- [2] Lei A, Kang N, Zhao Y, Liu H, An H, Xiong J, Wang R, Xie Z, Tu Y, Xu G, Zhou X, Fang Z, Wang W, Xia L, Feng W, Zhao X, Ji L, Cui Y, Zhou S, Liu Z, Zheng C, Wang L, Gao Y, Huang X and Fu S 2024 Physical Review Letters 132 035102
- [3] Wang P, An H, Fang Z, Xiong J, Xie Z, Wang C, He Z, Jia G, Wang R, Zheng S, Xia L, Feng W, Shi H, Wang W, Sun J, Gao Y and Fu S 2024 Matter and Radiation at Extremes 9 015602
- [4] Kanstein C, Wasser F, Zahter S, Atzeni S, Benincasa G, Cristoforetti G, Erdogdu G, Fischer M, Gizzi L A, Glize K, Grimm S J, Hornung J, Hume E, Koester P, Kuschel S, Meffert T, Neufeld F, Neumayer P, Nguyen K L, Theobald W, Winter V, Woolsey N, Zarrouk K, Zhao X, Bagnoud V and Roth M 2025 Plasma Physics and Controlled Fusion
- [5] Zhao Y, Yin H, Zhao B and Cui Z 2024 Nuclear Fusion 64 016022
- [6] Liu Z, Ma H, Wang W, Li X, Wang P, Wang C, Yew S, Weng S, Sheng Z and Zhang J 2023 Nuclear Fusion 63 126010
- [7] Bates J W, Follett R K, Shaw J G, Obenschain S P, Myatt J F, Weaver J L, Wolford M F, Kehne D M, Myers M C and Kessler T J 2023 Physics of Plasmas 30 052703
- [8] Yin H, Zhao Y, Zhao B and Shen B 2025 Plasma Physics and Controlled Fusion 67 045022

- [9] Seaton A G, Yin L, Follett R K, Albright B J and Le A 2022 Physics of Plasmas 29 042707
- [10] Li X, Qiu J, Hao L and Zou S 2025 Investigation of stimulated brillouin scattering driven by broadband lasers in high-z plasmas (*Preprint* 2511.11395) URL https://arxiv.org/abs/2511.11395
- [11] Michel P 2023 Introduction to Laser-Plasma Interactions Graduate Texts in Physics (Cham: Springer International Publishing) ISBN 978-3-031-23423-1 978-3-031-23424-8
- [12] Arber T D, Bennett K, Brady C S, Lawrence-Douglas A, Ramsay M G, Sircombe N J, Gillies P, Evans R G, Schmitz H, Bell A R and Ridgers C P 2015 Plasma Physics and Controlled Fusion 57 113001 ISSN 0741-3335, 1361-6587
- [13] Nanbu K and Yonemura S 1998 Journal of Computational Physics 145 639–654 ISSN 00219991
- [14] Sentoku Y and Kemp A 2008 Journal of Computational Physics 227 6846–6861 ISSN 00219991
- [15] Roden J A and Gedney S D 2000 Microwave and Optical Technology Letters 27 334–339
- [16] Liu Q K, Zhang E H, Zhang W S, Cai H B, Gao Y Q, Wang Q and Zhu S P 2022 Physics of Plasmas 29 102105
- [17] Yao C, Li J, Hao L, Yan R, Wang C, Lei A, Ding Y K and Zheng J 2024 Nuclear Fusion 64 106013
- [18] Zhao Y, Lei A, Kang N, Li F, Li X, Liu H, Lin Z, Yin H, Xu Y, Yi Y and Xu Z 2024 Physical Review E 110 065206
- [19] Langdon A B 1980 Physical Review Letters 44 575–579 ISSN 0031-9007
- [20] Qiu J, Hao L, Cao L and Zou S 2021 Plasma Physics and Controlled Fusion 63 125021 ISSN 0741-3335, 1361-6587
- [21] Beresnyak A 2023 NRL Plasma Formulary U.S. Naval Research Laboratory
- [22] Mandel L and Wolf E 1962 Proceedings of the Physical Society ${\bf 80}$ 894
- [23] Lei Z, Zhang Y, Song T, Wang Q, Yuan W, Ren K, Huang C, Zhao Y, Qing B, Zhang Z, Yang G, Li Y, Chen T, Che X, Zhu T, Xiong G, Lv M, Zhao Y, Li L, Wang L, Li J, Zhang J, Qiao B and Yang J 2025 Nuclear Fusion 65 066015
- [24] Shestakov A I, Prasad M K, Milovich J L, Gentile N A, Painter J F and Furnish G 2000 Comput. Methods Appl. Mech. Engrq.